J. Phys. Chem. A **2002,** *106,* 10525−10531

Vibrational Spectrum and Structure of the Fe_2CO Molecule. An Infrared Matrix Isolation and Density Functional Theory Study

Benoît Tremblay,*,† Gennady Gutsev,‡ Laurent Manceron,† and Lester Andrews‡

LADIR/Spectrochimie Moléculaire CNRS UMR 7075- Université Pierre et Marie Curie, case 49,
4 place Jussieu 75252 Paris, France, and Department of Chemistry, University of Virginia, Box 400319,
Charlottesville, Virginia 22901-4319

Received: July 20, 2002; In Final Form: September 10, 2002

The Fe_2 + CO reaction has been reinvestigated using deposition of ground-state iron atoms and carbon monoxide in solid argon. The iron carbonyl products observed without activation energy are Fe_2CO and higher carbonyl species $Fe(CO)_x$. The Fe_2CO molecule has been characterized through the observation of four fundamental transitions assigned to the three stretching (ν_1, ν_2, and ν_4) and the highest frequency bending vibration (ν_3). Isotopic data on ν_1, ν_2, ν_3, ν_4, $\nu_1 + \nu_2$, and $2\nu_1$ have been measured in the near- and far-infrared regions. From the experimental data, a linear structure can be excluded and precise C−O, Fe−C, and Fe−Fe bond force constants can be determined. Geometrical and electronic configurations of the lowest energy states for each possible spin multiplicity of Fe_2CO, Fe_2CO^-, and Fe_2CO^+ have been calculated using density functional theory with the generalized approximation for the exchange-correlation functional (DFT-GGA). The calculation results also predict an end-on, but highly bent, Fe−Fe−C−O ground-state structure for the neutral species ($^7A'$). Comparison of the DFT force field computed harmonic frequencies with the experimental frequencies obtained for Fe_2CO isolated in solid argon show a very good agreement, which validates the ground-state DFT prediction. Computed ionization energies and electron affinities are also reported, along with the vibrational harmonic frequencies for the predicted ionic ground states.

I. Introduction

The central role played by the CO molecule in chemisorption and catalysis or organometallic chemistry has motivated numerous experimental and theoretical studies on mono and small polynuclear transition metal (TM) complexes. With the goal of exploring structural, electronic, or chemisorption characteristics, workers nowadays are using surface science techniques and CO as a probe to study ultrasmall transition metal particles[1,2] or clusters[2] in order to bring insight on the catalytic activity of supported metal centers. When the size of a metal cluster decreases below a certain size, their properties are likely influenced by the nature of the support, but reliable data on the isolated particles are needed for comparison.

In recent years, the discovery and identification of multiwalled[4] and later single-walled[5,6] carbon nanotubes (SWNT) and their potential impact in technology has generated an enormous interest. The major technological requirement still to be met is the ability to grow large amounts of carbon nanotubes possessing selected properties. To produce SWNTs, Rao and co-workers have applied the direct pyrolysis of metallocenes $M(C_5H_5)_2$ (M = Fe, Co, and Ni) and $Fe(CO)_5$-acetylene mixtures.[7,8] Another process of the SWNT production is based on the use of gas-phase reactors in the presence of proper catalysts. Dresselhaus and co-workers have produced carbon nanotubes in a heated flow of benzene and ferrocene.[9] Recently, Smalley and co-workers have developed a high-pressure high-temperature process in which CO serves as carbon feedstock while $Fe(CO)_5$ decomposes to form iron clusters catalizing the growth of single-walled carbon nanotubes.[10] This is a complex kinetic process,[11] and the mechanism of metal-catalytic growth of carbon nanotubes presents a heavily debated issue.[12]

To gain insight into catalytic properties of iron clusters, one needs to know the structure and energetics of $Fe_n(CO)_kC_m$ clusters. Computations of transition metal compounds are, however, known to be very demanding and require reliable experimental data on isolated species for comparison and calibration. Considerable attention has been given to TM carbonyl triatomics, (see a recent review[13] and references therein), but much less is known about the structure and properties of the M_xCO species. Theoretical studies have been performed for Fe_2CO[14], Cu_2CO[15], Cu_3CO,[15] or Ni_2CO.[16] Other theoretical efforts have mainly focused on interactions of CO with surfaces of Ni, Fe, and Cu of different morphology which were modeled by M_n + CO clusters with assumed M_n geometries.[17,18]

Experimentally, the matrix isolation technique has been applied early to the characterization of unsaturated binary $M(CO)_x$ ($x = 1-4$, 5, or 6) transition metal carbonyls.[20] When annealing the sample to promote aggregation or using high a metal/rare gas ratio, polynuclear metal carbonyls are formed, but a clear identification can be very difficult because a large number of species appear in the spectrum.[21] Concerning the smallest iron carbonyls, the FeCO species was first reported by Ozin and Moskovits by reaction of ground state thermal Fe atoms and carbon monoxide molecules in solid argon and identified as the carrier of an absorption at 1898 cm^{-1}.[20] In comparable experimental conditions, Peden and co-workers have assigned the same band to FeCO, and at higher iron concentra-

---

* To whom correspondence should be addressed. Fax: 33-1-44273021. E-mail: tremblay@ccr.jussieu.fr.

† Université Pierre et Marie Curie.

‡ University of Virginia.

10.1021/jp026573a CCC: $22.00

tion in solid krypton, a band at 1923 cm^{-1} was assigned to the C−O stretch of Fe_2CO.[22]

Recently, Zhou and Andrews reinvestigated the Fe + CO reaction using laser-ablated Fe atoms and carbon monoxide in argon and neon matrixes.[23,24] In argon, these authors reassigned the IR band near 1898 cm^{-1} to the diiron monocarbonyl molecule Fe_2CO and assigned a band at 1922.0 cm^{-1}, with notably different isotopic effects, to the monoiron monocarbonyl molecule FeCO. Finally, in the gas phase, the FeCO ground state ν_1 vibrational transition could be derived from the photodetachment spectrum of $FeCO^-$ and estimated at 1950 ± 10 cm^{-1}.[25] Later, diode laser spectroscopic studies of the iron carbonyl radical FeCO generated by ultraviolet laser photolysis of $Fe(CO)_5$ have been performed, and the C−O stretching band origin was measured at 1948.98 or 1946.47 cm^{-1} in two separate studies.[26,27]

We report here new data concerning the stretching and bending vibrations ν_1, ν_2, ν_3, and ν_4, for several isotopic species (using $^{12}C^{16}O$, $^{13}C^{16}O$, and $^{12}C^{18}O$ isotopic precursors for CO) of Fe_2CO isolated in solid argon. Observations of overtone and binary combination levels in the near-infrared are also reported. DFT calculations of the geometrical and electronic properties of the Fe_2CO molecule are presented and compared to the experimental values. Comparisons with bond force constants of CoCO,[28] NiCO,[29,30] and CuCO[31] are also presented.

II. Computational and Experimental Procedures

A. Theoretical Methods. Our calculations are performed using the density-functional theory (DFT)[32] where linear combinations of atomic orbitals constitute one-electron Kohn−Sham orbitals. A generalized gradient approximation consisting of the combination of Becke's exchange[33] and Perdew-Wang's correlation functionals,[34] referred to as BPW91, is chosen for the exchange-correlation functional. The Gaussian 98 program[35] was used. We should note that replacing the correlation part by the Lee−Yang−Parr (LYP)[36] correlation functional yields vibrational frequencies in poorer agreement with the experimental values than using Perdew-Wang's correlation functional, unlike what was found in other cases such as 3d-metal monoxides,[37] monocarbides,[38] and the CO_2 dimer.[39]

For the atomic orbitals, we have used the standard[40−43] 6-311+G* basis (Fe, [10s7p4d1f]; O, [5s4p1d]). Geometry optimizations were carried out by the steepest descent method until the gradient forces fell below the threshold value of 3×10^{-4}. Subsequent analytical harmonic frequency calculations were performed in order to confirm that the optimized geometries correspond to stationary states. Optimizations were performed for each possible spin multiplicity of Fe_2CO, Fe_2CO^-, and Fe_2CO^+ until further increasing the spin multiplicity would result in a state unstable toward dissociation to the ground states $Fe_2^{0,+,-}$ and CO.

B. Experimental Procedures. Experimental procedures and methods were the same as those used in ref 44. The Fe_2CO molecules were prepared by co-condensing iron vapor and dilute CO−Ar mixtures (0.5 to 2% CO in Ar) onto a flat, highly polished, Ni-plated copper mirror maintained at ca. 10 K using a closed-cycle cryogenerator, situated in a stainless steel cell evacuated at a base pressure less than 5×10^{-7} mbar, before refrigeration of the sample holder. A tungsten filament, mounted in a furnace assembly and wetted with iron (Alpha Inorganics, 99.9965%) was heated from 1200 to 1400 °C to generate the Fe vapor. The metal deposition rate was carefully monitored with the aid of a quartz microbalance and was typically of the order of about 0.05 to 1.3 μg/min.

High-purity argon (Prodair, 99.995%) and carbon monoxide (Matheson; 99.5%) ^{13}CO (CEA, Saclay, France, 99% ^{13}CO including 8% $^{13}C^{18}O$) and $^{12}C^{18}O$ (MSD; 98% ^{18}O) were used to prepare the CO−Ar mixtures after removing condensable impurities with a liquid nitrogen trap.

In general, after deposition times varied between 20 and 90 min, infrared spectra of the resulting sample were recorded in the transmission-reflection mode between 5000 and 70 cm^{-1} using a Bruker 120 FTIR spectrometer and suitable combinations of CaF_2/Si, KBr/Ge or 6 μm Mylar beam splitters with either liquid-N_2-cooled InSb or narrow band HgCdTe photodiodes or a liquid-He-cooled Si−B bolometer, fitted with cooled band-pass filters. The spectra were recorded at 0.5 cm^{-1} resolution. Bare mirror backgrounds, recorded at 10 K from 5000 to 70 cm^{-1} prior to sample deposition, were used as references in processing the sample spectra. Also, absorption spectra in the near-, mid-, and far-infrared were collected on the *same* samples through either CaF_2, CsI, or polyethylene windows mounted on a rotatable flange separating the interferometer vacuum (10^{-3} mbar) from that of the cryostatic cell (10^{-7} mbar). The spectra were subsequently subjected to baseline correction to compensate for infrared light scattering and interference patterns.

The sample was next irradiated, typically between 30 and 60 min, using a tungsten lamp and a 700 nm highpass filter or a 200 W mercury−xenon high-pressure arc lamp and broad band-pass filter between 420 and 260 nm. Infrared spectra of the photolyzed or annealed samples were recorded between 5000 and 70 cm^{-1} as outlined above.

III. Results and Discussion

A. Electronic and Geometric Structure from Theoretical Calculations. The ground state of atomic iron is ^5F and has the $3d^64s^2$ electronic configuration. Attachment of the second iron atom leads to an increase in spin multiplicity, and the Fe_2 dimer has[45−55] a $^7\Delta_u$ ground state, whereas attachment of carbon monoxide leads to a decrease in the spin multiplicity and the ground state of FeCO is $^3\Sigma^-$.[26] Siegbahn found a planar $^{11}B_2$ state of Fe_2CO at the Hartree−Fock level of theory, having mentioned that his high-level averaged-coupled pair functional calculations did not converge.[14] The C−O frequency in this state was calculated to be 1199 cm^{-1}, which is definitely very low compared to experimentally observed C−O frequencies in transition metal carbonyls.[13]

All geometrical configurations of the lowest energy states optimized at the BPW91 level for each possible spin multiplicity of neutral and ionic Fe_2CO states are planar (Figure 1). Some geometry optimizations were performed starting with nonplanar trial geometries without imposing any symmetry constraint. However, all of them reverted to the planar configurations. All states optimized possess C_s symmetry with nonequal C−Fe_1 and C−Fe_2 distances, except $^{10}B_2$ of the Fe_2CO^- anion.

The ground state of Fe_2CO is calculated to be $^7A'$ with an end-on structure, relatively close to that of the ground state of Fe_2CO^- ($^6A'$), but the ground state of Fe_2CO^+ is $^6A'$ with a the carbon atom bridging the Fe−Fe bond (see Figure 1). The ion spin multiplicities are in compliance with an empirical "±1" rule according to which the spin multiplicities of the ground state of a neutral and the ground states of its singly charged ions may differ by ±1. The lowest $^7A''$ state of Fe_2CO is above its ground state by 0.31 eV and also presents an end-on configuration but with a smaller Fe−Fe−C bond angle of 96°. Harmonic frequencies computed for the naturally occurring most abundant $^{56}Fe_2{}^{12}C^{16}O$ along with isotopic species $^{56}Fe_2{}^{13}C^{16}O$,

TABLE 1: Computed Vibrational Frequencies (in cm^{-1}) at the BPW91 Level of Ground-State Fe_2CO, Fe_2CO^-, and Fe_2CO^+ for Some Isotopic Species[a]

	A′	A′	A″	A′	A′	A′
$^{56}Fe_2{}^{12}C^{16}O$	52 [2]	253 [15]	303 [0]	338 [7]	471 [21]	1929 [1152]
$^{56}Fe_2{}^{13}C^{16}O$	54 [2]	252 [15]	280 [0]	312 [4]	468 [25]	1876 [1033]
$^{56}Fe_2{}^{12}C^{18}O$	54 [2]	252 [16]	273 [0]	303 [3]	464 [27]	1870 [1002]
$^{56}Fe_2{}^{12}C^{16}O^+$	217 [0]	228 [13]	320 [1]	335 [1]	490 [1]	1889 [465]
$^{56}Fe_2{}^{13}C^{16}O^+$	211 [6]	231 [1]	311 [1]	319 [0]	487 [1]	1841 [397]
$^{56}Fe_2{}^{12}C^{18}O^+$	202 [6]	237 [1]	302 [1]	318 [0]	482 [1]	1836 [388]
$^{56}Fe_2{}^{12}C^{16}O^-$	73 [2]	311 [3]	355 [1]	380 [41]	543 [1]	1784 [1282]

[a] IR absolute intensities (km/mol) are given in brackets.

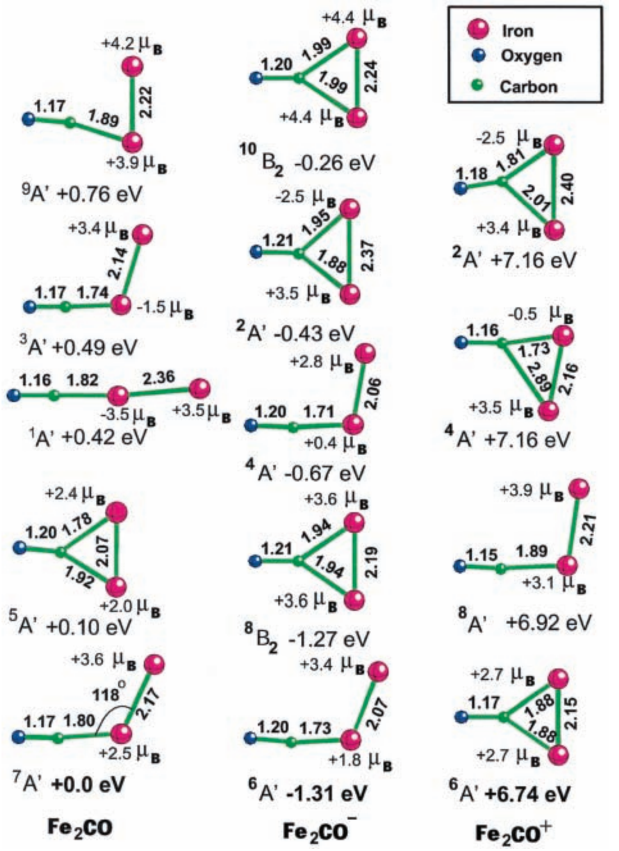

Figure 1. Geometrical configurations of the lowest energy states for each possible spin multiplicity of Fe_2CO, Fe_2CO^-, and Fe_2CO^+. Bond lenghts are in angstroms, and magnetic moments at iron sites are in Bohr magnetons.

$^{56}Fe_2{}^{12}C^{18}O$, and $^{56}Fe_2{}^{13}C^{18}O$ are presented in Table 1 together with the IR intensities. The lowest energy bridged configuration of Fe_2CO belongs to $^5A'$, which is only 0.1 eV above the ground state. The predicted vibrational frequencies are 219[1], 304[10] (Fe−C), 335[2] (Fe−Fe), 379[5](A″), 541[0] (Fe−C), and 1764[609] (C−O) cm^{-1} [IR intensities in km/mol] and notably different from those computed for the $^7A'$ state, and thus vibrational data will constitute an adequate test. The BLYP/6-311+G* approach also predicts $^7A'$ to be the ground state of Fe_2CO but increases the Fe−Fe−C bond angle to 126°. Correspondingly, the BLYP vibrational frequencies are in worse agreement with experiment (see Table 3) than those computed at the BPW91 level.

It is interesting to compare the Fe_2CO molecular parameters to those of Fe_2 ($^7\Delta_u$, $r_e = 2.01$ Å, $\omega_e = 397$ cm^{-1}) and CO ($^1\Sigma^+$, $r_e = 1.14$ Å, $\omega_e = 2127$ cm^{-1}) computed at the same BPW91/6-311+G* level. The Fe−Fe and C−O bond lengths do elongate by 0.16 and 0.03 Å, respectively, whereas Fe−Fe and C−O stretching frequencies decrease by 144 (−36%) and 200 (−9%) cm^{-1}, respectively. The computed Fe_2−CO bond strength is 1.38 eV (32 kcal/mol).

TABLE 2: Vibrational Frequencies[a] and Relative Intensities of the IR Absorption Bands Observed for Various Isotopic Species of Fe_2CO

$Fe_2{}^{12}C^{16}O$	$Fe_2{}^{13}C^{16}O$	$Fe_2{}^{12}C^{18}O$	assignment
3770.8 [0.8]	3684.8	3687.5	$2\nu_1$
2381.6 [0.03]	2333.3	n.o.[c]	$\nu_1 + \nu_2$
1898.0 [100]	1854.5	1855.7	ν_1
483.2 [0.9]	477.8	471.1	ν_2
371.6 [0.4]	361.2	368.1	ν_3
291.5 [0.6]	290.7	291.2	ν_4

[a] Vibrational frequencies in cm^{-1}. The values quoted are within ± 0.1 cm^{-1}. [b] Relative IR intensities with respect to ν_1. [c] Not observed.

TABLE 3: Comparison of the Experimental Vibrational Frequencies of Fe_2CO Isolated in Solid Argon with the DFT Harmonic Frequencies

	ν_1	ν_2	ν_3	ν_6	ν_4	ν_5
exp	1898.0[a] [1000][b]	483.2 [9]	371.6 [4]	n.o.[c]	291.5 [6]	n.o.
BPW91	1929 [1229][d]	468 [26]	337 [7]	306 [0.2]	250 [21]	51 [1.5]
BLYP	1920 [1214]	429 [27]	314 [1]	284 [0]	253 [19]	44 [1]

[a] The frequency corrected for harmonicity is $\omega_1 = 1923 \pm 5$ (see text). [b] Relative IR intensities with respect to ν_1. The ν_1 intensity is here arbitrary set to 1000. [c] Not observed. [d] Calculated absolute IR intensities (in km/mol).

As is seen in Figure 1, there is a number of low-lying states very close to the ground state of either neutral or ionic species. The low-spin states have antiferromagnetic couplings of magnetic moments at iron sites which is in agreement with the antiferromagnetic coupling in the singlet and triplet states of the Fe_2[54,55] and Co_2[39] dimers. The computed adiabatic electron affinity of Fe_2CO, 1.31 eV, is somewhat larger than the adiabatic electron affinities of both Fe_2 (BPW91, 0.94 eV;[56]experiment, 0.902 ± 0.008 eV[57]) and FeCO (BPW91, 0.97 eV;[58] experiment, 1.157 ± 0.005 eV[25]). The computed adiabatic ionization potential of Fe_2CO, 6.74 eV, is fairly close to that of Fe_2 (BPW91, 6.68 eV;[55] experiment, 6.30 ± 0.01 eV[59]) and FeCO (BPW91, 7.07 eV;[58] experiment, 6.66 ± 0.17 eV[60]).

B. Experimental Results. Fe vapor was condensed with relatively dilute mixtures of CO in argon (0.25−3/100) at about 9 K to favor formation of monocarbonyls, FeCO and Fe_2CO. In the CO stretching region, the only range covered in the earlier studies, the products are very strongly absorbing and the reactant concentrations can be varied over 1 (for CO) or 2 (for Fe) orders of magnitude. The infrared spectrum of the products obtained after deposition of iron atoms, with an Fe/Ar ratio of 0.2/100, co-deposited with 2% CO in argon is shown in Figure 2. After deposition, several absorptions at 1948.6, 1935.6, 1898.0, 1879.5, and 1872.6 cm^{-1} were observed. The first four were assigned in a recent work to Fe_3CO, $Fe(CO)_3$, Fe_2CO, and

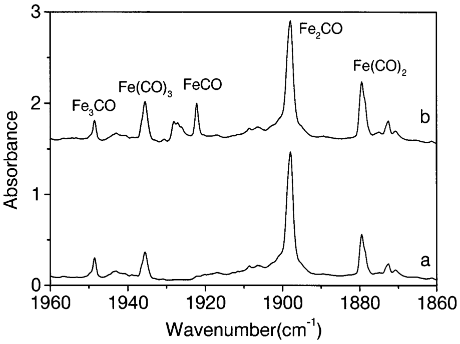

Figure 2. Infrared spectra in the CO stretching region for iron atoms co-deposited with 2% CO in argon. (a) After sample deposition; (b) after infrared irradiation with a 700−2000 nm band-pass filter.

$Fe(CO)_2$, respectively, whereas the last two bands correspond to the same molecule in two different trapping sites.[23]

Also, a weak band at 2132.9 cm^{-1} on the low-frequency side of unreacted CO (not shown here) appeared with a linear dependence with respect to either CO or iron concentration. The assignment of this band at 2132.9 cm^{-1} to a weakly bound van der Waals complex between an iron atom and a CO molecule in their ground states will be detailed in a forthcoming paper.[61]

When the sample was next irradiated with near-IR light to promote Fe atoms to either one of the first two excited ^5D or ^3D states, a new band appeared at 1922.0 cm^{-1}, and the bands at 1935.6 cm^{-1} ($Fe(CO)_3$) and 1879.5 cm^{-1} ($Fe(CO)_2$) increased, whereas the van der Waals complex at 2132.9 cm^{-1} is partially destroyed. The band at 1922.0 cm^{-1} was assigned to the monocarbonyl FeCO molecule in ref 23. This result then indicates that the FeCO molecule is not formed directly from ground-state reagents. Indeed, it was not observed in the previous study using thermal iron atoms, all of this implies that the experimental conditions specific to the laser-ablation experiments are necessary for the observation of FeCO; that is, excited-state reaction or photochemistry plays a crucial role in the reaction.[61] Because the interaction between the ground-state Fe atom and the CO molecule is not reactive, the formation of Fe_2CO could either result from the addition of a second Fe atom to the Fe···CO van der Waals complex or to the direct reaction of Fe_2 with CO. Recently, we found a similar situation for the formation of the CoCO and the Co_2CO molecules.[28] Now, we shall focus the rest of the discussion on the Fe_2CO molecule.

After studying the variations of the 1935.6, 1898.0, and 1879.5 cm^{-1} bands over a wide concentration range, this study confirms that these have third-, first-, and second-order dependence, respectively, with regard to the CO concentration. Varying the iron concentration, however, the bands at 1935.6 and 1879.5 cm^{-1} were observed to possess a first-order dependence, whereas the band at 1898.0 cm^{-1} has a quadratic dependence (Figure 3). With these considerations, we can confirm the assignment of this latter band to Fe_2CO, in agreement with previous results.[23]

After Fe/CO/Ar = 0.15/1/100 sample deposition at 10 K, the main band at 1898 cm^{-1} corresponds to the Fe_2CO species (Figures 4a and 5). Annealing at 25 K increased the 1898 band and produced a weak band at 1909.5 cm^{-1} (Figure 4b), assigned to $Fe_2(CO)_2$ in ref 23. Photolysis using 260−420 nm light greatly decreased the 1898 cm^{-1} band (Figure 4c), showing that the Fe_2CO species presents an electronic transition in the 3−5 eV range. Several new absorptions appeared both in the near- and far-infrared regions (Figure 6). Among these, five absorptions near 291, 371, 483, 2381, and 3771 cm^{-1} are always correlated and also presented a first-order relative intensity dependence with respect to the carbon monoxide concentration and a second-order dependence with respect to the metal. They also always behaved, upon matrix warm-up or UV irradiation, similarly to the strong band at 1898.0 cm^{-1}. This shows that all of these absorptions belong to the same species, i.e., Fe_2CO.

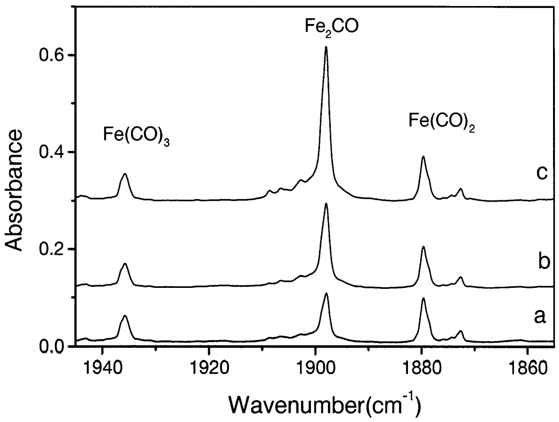

Figure 3. Infrared spectra of the Fe_2CO molecule in the CO stretching region: an iron concentration study with a 1% CO/Ar mixture. From bottom to top: Fe/CO/Ar = 0.05/1/100; Fe/CO/Ar = 0.09/1/100, absorbance scale ×0.5; Fe/CO/Ar = 0.14/1/100, absorbance scale ×0.35.

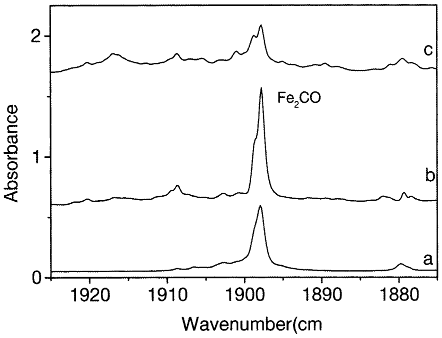

Figure 4. Infrared spectra in the CO stretching region for iron atoms co-deposited with 1% CO in argon. (a) After sample deposition at 10 K; (b) after annealing to 25 K; (c) after 420−260 nm irradiation.

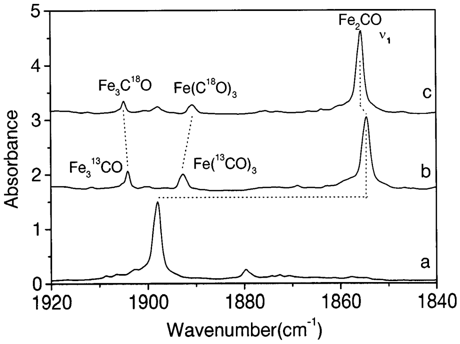

Figure 5. Infrared spectra of the Fe_2CO molecule in the CO stretching region for various isotopic precursors. (a) Fe + CO, (b) Fe + ^{13}CO, and (c) Fe + $C^{18}O$. In all samples, the Fe/CO/Ar molar ratios are approximately the same: 0.05/2/100.

The experiments were repeated using isotopically labeled CO, more specifically $^{13}C^{16}O$ and $^{12}C^{18}O$. The results of the isotopic study are presented in Figures 5 and 6 and Table 2. In the CO stretching region (Figure 5), the Fe_2CO band at 1898.0 cm^{-1} shifts to 1854.5 and 1855.7 cm^{-1} when $^{12}C^{16}O$ is replaced by $^{13}C^{16}O$ and $^{12}C^{18}O$, respectively. Similarly, in the far IR region, isotopic substitution causes the bands at 483.2, 371.6, and 291.5 cm^{-1} to shift (Figure 6). More specifically, the band at 483.2

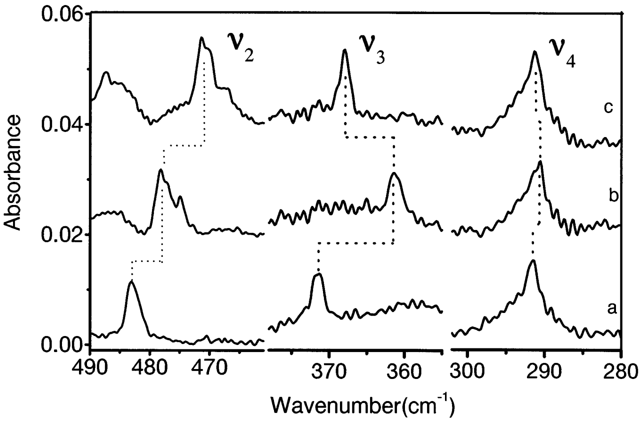

Figure 6. Infrared spectra of the Fe_2CO molecule in the low-frequency stretching mode Fe−C(ν_2), the bending mode (ν_3), and the stretching mode Fe−Fe (ν_4) regions for various isotopic precursors. (a) Fe + CO, (b) Fe + ^{13}CO, and (c) Fe + $C^{18}O$.

cm^{-1} shifts to 477.8 and 471.1 cm^{-1} upon replacing $^{12}C^{16}O$ by $^{13}C^{16}O$ and $^{12}C^{18}O$, respectively, whereas the absorption at 371.6 cm^{-1} shifts to 361.2 and 368.1 cm^{-1}, and the absorption at 291.5 cm^{-1} shifts to 290.7 and 291.2 cm^{-1}, with these same precursors.

The feature at 3770.8 cm^{-1}, at about twice the CO stretching frequency, shifts to 3684.8 and 3687.5 cm^{-1} when $^{13}C^{16}O$ and $^{12}C^{18}O$ are substituted for $^{12}C^{16}O$. The feature at 2381.6 cm^{-1}, consistent with the combination of the CO stretching mode at 1898.0 cm^{-1} and the mode at 483.2 cm^{-1}, shifts to 2333.3 cm^{-1} when $^{12}C^{16}O$ is replaced by $^{13}C^{16}O$. With the $^{12}C^{18}O$ isotope, the counterpart of the band at 2381.6 cm^{-1} has not been observed. This band is then expected around $(1855.7 + 471.1) = 2327$ cm^{-1}, which is very close to the strong absorption of the $C^{18}O_2$ molecule around 2320 cm^{-1} present as an impurity in our $^{12}C^{18}O$ sample.

The IR intensity measurements required special care, as the species presents both very strong and very weak absorptions in different spectral domains. Care was taken, to make measurements on the *same* samples in the various spectral ranges, and second to repeat these measures on optically thin and thick samples in order to avoid significant photometric errors. The values reported in Table 2 are relative intensities normalized with respect to the strongest fundamental, at 1898.0 cm^{-1}.

C. Vibrational Analysis and Comparison to the Theoretical Calculations. The positions of six absorption bands belonging to Fe_2CO isolated in solid argon have been clearly established. Two of these six are very weak, located above the strong carbonyl stretching absorption, ν_1, and are therefore likely to be either overtone or combination levels.

For the band observed at 1898.0 cm^{-1}, assignment to the ν_1 CO stretching vibration of Fe_2CO is straightforward, but the isotopic effects are interesting to analyze in more detail. Thus, ν_1 shifts to lower frequency by 43.5 cm^{-1} when $^{13}C^{16}O$ is used and by 42.3 cm^{-1} in the case of $^{12}C^{18}O$. The ν_1 frequency for $Fe_2{}^{12}C^{18}O$ is larger than that for $Fe_2{}^{13}C^{16}O$ even though the corresponding isolated CO oscillator possesses a smaller reduced mass. This indicates a substantial vibrational coupling between the CO and FeC coordinates which must be taken into account for an accurate discussion of the molecular parameters. The difference between the $^{16}O/^{18}O$ and $^{12}C/^{13}C$ isotopic shifts for an isolated CO oscillator (+3.83 cm^{-1}) and those actually observed for the metal carbonyl molecule (−1.2 cm^{-1} for Fe_2CO) constitutes an alternative, although indirect, indication of the metal−ligand bond strength. In the related NiCO species[30] in which the metal−CO coordination binding is large, this difference reaches $41.0 - 47.9 = -6.9$ cm^{-1}. For CuCO,[31] with a much weaker metal−ligand interaction, this difference is +3.5 cm^{-1}, virtually that for an isolated CO oscillator, despite similar ν_1 mode frequencies.

The band observed at 3770.8 cm^{-1} is consistent with a $2\nu_1$ overtone. For $Fe^{12}C^{16}O$, $2 \times \nu_1 = 2 \times 1898.0$ or 3796.0 cm^{-1}, which represents a X_{11} anharmonicity constant of −12.2 cm^{-1}. The $^{12}C/^{13}C$ and $^{16}O/^{18}O$ shifts for this overtone support this assignment, as the isotope shifts are very nearly twice those observed for the ν_1 fundamental.

The expected effect on the low-frequency Fe−CO stretching mode when $^{12}C^{16}O$ is substituted by $^{13}C^{16}O$ and $^{12}C^{18}O$ would result in increasing shifts ($\Delta\nu$) to lower frequencies. Furthermore, it is expected that $\Delta\nu(Fe^{12}C^{18}O) > \Delta\nu(Fe^{13}C^{16}O)$. This is what is observed for the band at 483.2 cm^{-1}, and we have assigned this band to the ν_2 stretching mode of Fe_2CO.

From their positions and isotopic shifts, the weaker absorption observed at 2381.6 cm^{-1} for $Fe^{12}C^{16}O$ is assigned to a combination band. Indeed, $\nu_1 + \nu_2 = 1898.0 + 483.2$ or 2381.2 cm^{-1} which represents $X_{12} = +0.4$ cm^{-1} anharmonicity. The other possible binary levels involving ν_1 were not observed in this study, but from the X_{11} and X_{12} values deduced here and comparisons with other metal carbonyl molecules, a $\omega_1 = 1923 \pm 5$ cm^{-1} harmonic frequency value can be proposed, in very good agreement with the DFT-calculated value.

For a bending vibration associated with a linear (or close to linear) Fe−C−O group, substitution of $^{12}C^{16}O$ by $^{13}C^{16}O$ should cause a much larger shift to lower frequencies than substitution by $^{12}C^{18}O$. This trend is observed for the band at 371.6 cm^{-1}. In fact, isotopic substitution caused the band to shift by −10.4 cm^{-1} for $Fe^{13}C^{16}O$ and −3.5 cm^{-1} for $Fe^{12}C^{18}O$. The band at 371.6 cm^{-1} must therefore be assigned to an Fe−C≡O bending mode within Fe_2CO (ν_3).

The nature of the fourth observed transition, near 291 cm^{-1}, is less straightforward to establish. According to the DFT results presented before, two fundamental vibrations should be located in this energy range, and both are possible candidates for this transition. These correspond to the out-of-plane bending mode (ν_6, A″ symmetry) calculated near 303 cm^{-1} and the remaining in-plane A′ symmetry mode, ν_4, near 253 cm^{-1}. The very small $^{16}O/^{18}O$ and $^{12}C/^{13}C$ isotopic shifts observed for this absorption rule out the first possibility or any other involving substantially the carbonyl group. Assignment to the ν_4 fundamental, best described as involving mainly the Fe−Fe stretching coordinate, is indicated (Table 1).

To test further these assignments and help quantitative comparisons with other related systems, the harmonic force field was refined using the experimental isotopic effects. More specifically, we first searched for the set of harmonic force constants which would best reproduce the observed isotopic shifts for Fe_2CO with the DFT-calculated geometrical configuration, i.e., 1.80 Å for Fe−C, 2.17 Å for Fe−Fe, and 1.17 Å for C−O. The best fit between the calculated harmonic frequencies for the various isotopic forms of Fe_2CO and the experimental frequencies is presented in Table 4. The requirement of reproducing simultaneously all of the isotope effects on the ν_1 and ν_2 stretching modes imposes severe constraints on the form of the stretching normal coordinates, and the C−O and Fe−C bond and interaction force constants are quite precisely determined. Compared to other MCO triatomics analyzed within the same framework (Table 5), the CO bond force constants in FeCO and Fe_2CO are somewhat lower, in correspondence with earlier theoretical studies,[62,63] in which the weakening of the CO bond strength in monocarbonyls has been

TABLE 4: Comparison of the Experimental Frequencies and Calculated Harmonic Frequencies for the Various Isotopic Species of Fe_2CO (cm^{-1})

	$Fe_2{}^{12}C^{16}O$			$Fe_2{}^{13}C^{16}O$			$Fe_2{}^{12}C^{18}O$			$^{56}Fe^{54}Fe\,CO$	$^{54}Fe^{56}Fe\,CO$
	exp	calc	$\Delta\nu$ (exp-cal)	exp	calc	$\Delta\nu$ (exp-cal)	exp	calc	$\Delta\nu$ (exp-cal)	calc	calc
ν_1	1898.0	1898.0	0	1854.5	1853.8	0.7	1855.7	1855.2	0.5	1898.0	1898.0
ν_2	483.2	483.2	0	477.8	478.0	−0.2	471.1	471.1	0	483.7	486.5
ν_3	371.6	371.6	0	361.2	361.0	0.2	368.1	367.7	0.4	371.7	372.1
ν_4	291.5	291.5	0	290.7	290.8	−0.1	291.2	291.3	-0.1	294.3	293.7

[a] The force constants giving the best fit of the experimental data are $F_{FeC} = 2.70$ mdyn Å^{-1}, $F_{CO} = 14.57$ mdyn Å^{-1}, $F_{FeFe} = 1.53$ mdyn Å^{-1}, $F_{FeC,CO} = 0.80$ mdyn Å^{-1}, $F_{FeCO} = 0.378$ mdyn Å rad^{-2}.

TABLE 5: Comparison of Different Experimental Data for Fe_2CO, FeCO, CoCO, NiCO, and CuCO in Solid Argon

	F_{MC} (mdyn Å^{-1})	F_{CO} (mdyn Å^{-1})	$F_{MC,CO}$ (mdyn Å^{-1})	F_{MCO} (mdyn Å rad^{-2})	vibrational frequencies (cm^{-1})		
					ν_{CO}	ν_{MCO}	ν_{M-CO}
Fe_2CO	2.70	14.57	0.80	0.38	1898.0	371.6	483.2
FeCO	3.71	14.44	0.69	0.49	1922.2	431.2	568.7
CoCO	3.96	14.74	0.55	0.47	1957.5	424.9	579.2
NiCO	4.07	15.44	0.65	0.49	1994.5	409.1	591.1
CuCO	1.03	16.58	0.52	0.14	2010.3	322.7	207.5

related to the extent of the metal−CO π back donation. The metal−carbon bond force constant is however substantially smaller than for any MCO triatomics studied so far, except in the weakly bound CuCO system.

This calculation also shows that the expected ^{54}Fe isotope effects on ν_4 for the $^{54}Fe^{56}FeCO$ and $^{56}Fe^{54}FeCO$ satellite species, second in abundances to the main $^{56}Fe^{56}FeCO$ species (5/5/83), are quite small ($\approx$3 cm^{-1}). Given the line widths observed here in solid argon, such small shifts could not be resolved but are likely to contribute to the shoulder on the high-frequency side (Figure 6). The magnitudes of the small isotopic effects observed on the ν_4 transition demonstrate a small coupling of the Fe−Fe coordinate with another one. Coupling with the Fe−C stretching coordinate would result in $^{12}C/^{13}C$ and $^{16}O/^{18}O$ effects of increasing magnitudes, whereas the opposite is observed. This indicates a coupling with the Fe−C═O in-plane bending coordinate, a phenomenon which can only take place if the molecule is substantially bent out of linearity. Test calculations using the semiempirical harmonic potential defined in Table 4 show that for molecular geometries with Fe−Fe−C bond angle values greater than 140° the observed trend on the isotope effects could not be reproduced, in agreement with the theoretical BPW91 value of 118° presented earlier. The 1.53 mdyne/Å Fe−Fe bond force constant calculated here with the bent DFT geometry (Table 4) is very close to that found for the Fe_2 diatomics in comparable matrix isolation condition[64] (1.48 mdyne/Å), in contrast with the trend found here at the DFT-BPW91 level.

IV. Conclusions

The Fe_2CO species has been studied by a combination of cryosynthesis and IR absorption spectroscopy in solid argon, along with calculations using density functional theory with the generalized approximation for the exchange-correlation functional. Detailed isotopic studies and normal-mode analysis lead to the assignment of four fundamental transitions and two binary levels for an end-bound Fe_2CO species with a bent structure, in complete agreement with the optimized geometry obtained for the $^7A'$ ground state. DFT results are also presented for the five next low-lying excited states and for the $Fe_2CO^{+,-}$ species.Theoretical and experimental frequencies are in good agreement, with a largest difference of 40 cm^{-1} (found for the ν_4 mode). Comparisons are presented with related 3d-metal carbonyl triatomics.

Acknowledgment. This work was supported by NASA Grant No. NCC2-5415 and NSF Grant No. 00-78836 to L.A. and C.N.R.S. Grant UMR 7075 to the Université Pierre et Marie Curie. We thank Danielle Carrère for her competent assistance in the experimental work.

References and Notes

(1) Lambert, R. M.; Pacchioni, G. *Chemisorption and Reactivity on Supported Clusters and Thin Films*; Kluwer Academic Publishers: Dordrecht, 1997.

(2) Henry, C. R. *Surf. Sci. Rep.* **1998**, *31*, 231.

(3) Franck, M.; Kühnemuth, R.; Bäumer, M.; Freund, H. J. *Surf. Sci.* **2000**, *454*, 968.

(4) Iijima, S. *Nature* **1991**, *354*, 56.

(5) Iijima, S.; Ichihashi, T. *Nature* **1993**, *363*, 603.

(6) Bethune, D. S.; Kiang, C. H.; deVries, M. S.; Gorman, G.; Savoy, R.; Vazquez, J.; Beyers, R. *Nature* **1993**, *363*, 605.

(7) Sen, R.; Govindaraj, A.; Rao, C. N. R. *Chem. Phys. Lett.* **1997**, *267*, 276.

(8) Satishkumar, B. C.; Govindaraj, A.; Sen, R.; Rao, C. N. R. *Chem. Phys. Lett.* **1998**, *293*, 47.

(9) Cheng, H. M.; Li, F.; Sun, X.; Brown, S. D. M.; Pimenta, M. A.; Marucci, A.; Dresselhaus G.; Dresselhaus, M. S. *Chem. Phys. Lett.* **1998**, *289*, 602.

(10) Nikolaev, P.; Bronikowski, M. J.; Bradley, R. K.; Rohmund, F.; Colbert, D. T.; Smith, K. A.; Smalley, R. E. *Chem. Phys. Lett.* **1999**, *313*, 91.

(11) Dateo, C. E.; Gökçen, T.; Meyyappan, M. *J. Nanosci. Nanotech.* Submitted.

(12) Bronikowski, M. J.; Willis, P. A.; Colbert, D. T.; Smith, K. A.; Smalley, R. E. *J. Vac. Sci. Technol. A* **2001**, *19*, 1800.

(13) Zhou, M.; Andrews, L.; Bauschlicher, C. W. *Chem. Rev.* **2001**, *101*, 1931.

(14) Siebgahn, P. E. M. *J. Chem. Phys.* **1991**, *95*, 364.

(15) Fournier, R. *J. Chem. Phys.* **1995**, *102*, 5396.

(16) Ignatyev, I. S.; Schaefer, H. F.; King, R. B.; Brown, S. T. *J. Am. Chem. Soc.* **2000**, *122*, 1989.

(17) Meehan, T. E.; Head, J. D. *Surf. Sci.* **1991**, *L55*, 243.

(18) Görling, A.; Ackermann, L.; Lauber, J.; Knappe, P.; Rösch, N. *Surf. Sci.* **1993**, *286*, 26.

(19) Siegbahn, P. E. M. *Surf. Sci.* **1992**, *269*, 276.

(20) Ozin, G. A.; Moskovits, M. *Cryochemistry*; Wiley: New York, 1976; Chapter 8.

(21) Moskovits, M.; Hulse, J. E. *J. Phys. Chem.* **1977**, *81*, 2004.

(22) Peden, C. H. F.; Parker, S. F.; Barret, P. H.; Pearson, R. G. *J. Phys. Chem.* **1983**, *87*, 2329.

(23) Zhou, M.; Chertihin, G. V.; Andrews, L. *J. Chem. Phys.* **1998**, *109*, 10893.

(24) Zhou, M.; Andrews, L. *J. Chem. Phys.* **1999**, *110*, 10370.

(25) Villalta, P. W.; Leopold, D. G. *J. Chem. Phys.* **1993**, *98*, 7730.

(26) Tanaka, K.; Tachikawa, Y.; Tanaka, T. *Chem. Phys. Lett.* **1997**, *281*, 285.

(27) Tanaka, K.; Sakaguchi, K.; Tanaka, T. *J. Chem. Phys.* **1997**, *106*, 2118.

(28) Tremblay, B.; Alikhani, M. E.; Manceron, L. *J. Phys. Chem. A* **2001**, *105*, 11388.
(29) Joly, H. A.; Manceron, L. *Chem. Phys.* **1998**, *226*, 61.
(30) Manceron, L.; Alikhani, M. E. *Chem. Phys.* **1999**, *244*, 215.
(31) Tremblay, B.; Manceron, L. *Chem. Phys.* **1999**, *242*, 235.
(32) Kohn, W.; Sham, L. J. *Phys. Rev.* **1965**, *140*, A1133.
(33) Becke, A. D. *Phys. Rev. A* **1988**, *38*, 3098.
(34) Perdew, J. P.; Wang, Y. *Phys. Rev. B* **1991**, *45*, 13244.
(35) Frisch, M. J.; Trucks, G. W.; Schlegel, H. B.; Scuseria, G. E.; Robb, M. A.; Cheeseman, J. R.; Zakrzewski, V. G.; Montgomery, J. A., Jr.; Stratmann, R. E.; Burant, J. C.; Dapprich, S.; Millam, J. M.; Daniels, A. D.; Kudin, K. N.; Strain, M. C.; Farkas, O.; Tomasi, J.; Barone, V.; Cossi, M.; Cammi, R.; Mennucci, B.; Pomelli, C.; Adamo, C.; Clifford, S.; Ochterski, J.; Petersson, G. A.; Ayala, P. Y.; Cui, Q.; Morokuma, K.; Malick, D. K.; Rabuck, A. D.; Raghavachari, K.; Foresman, J. B.; Cioslowski, J.; Ortiz, J. V.; Stefanov, B. B.; Liu, G.; Liashenko, A.; Piskorz, P.; Komaromi, I.; Gomperts, R.; Martin, R. L.; Fox, D. J.; Keith, T.; Al-Laham, M. A.; Peng, C. Y.; Nanayakkara, A.; Gonzalez, C.; Challacombe, M.; Gill, P. M. W.; Johnson, B. G.; Chen, W.; Wong, M. W.; Andres, J. L.; Head-Gordon, M.; Replogle, E. S.; Pople, J. A. *Gaussian 98*, revision A.11; Gaussian, Inc.: Pittsburgh, PA, 1998.
(36) Lee, C.; Yang, W.; Parr, R. G. *Phys. Rev. B* **1988**, *37*, 785.
(37) Gutsev, G. L.; Rao, B. K.; Jena, P. *J. Phys. Chem. A* **2000**, *105*, 5374.
(38) Gutsev, G. L.; Andrews, L.; Bauschlicher, C. W., Jr. *Theor. Chem. Acc.* Submitted.
(39) Gutsev, G. L.; Khanna, S. N.; Jena, P. *Chem. Phys. Lett.* **2001**, *345*, 481.
(40) Frisch, M. J.; Pople, J. A.; Binkley, J. S. *J. Chem. Phys.* **1984**, *80*, 3265 and references therein.
(41) Wachters, A. J. H. *J. Chem. Phys.* **1970**, *52*, 1033.
(42) Hay, P. J. *J. Chem. Phys.* **1977**, *66*, 4377.
(43) Raghavachari, K.; Trucks, G. W. *J. Chem. Phys*. **1989**, *91*, 1062.
(44) Manceron, L.; Tremblay, B.; Alikhani, M. E. *J. Phys. Chem. A* **2000**, *104*, 3750.
(45) Harris, J.; Jones, R. O. *J. Chem. Phys.* **1979**, *70*, 830.
(46) Shim, I.; Gingerich, K. A. *J. Chem. Phys.* **1982**, *77*, 2490.
(47) Morse, M. D. *Chem. Rev.* **1986**, *86*, 1049.
(48) Salahub, D. R. In *Ab initio methods in Quantum Chemistry II*; Lawley, K. P., Ed.; Wiley: New York, 1987; pp 447−520.
(49) Dhar, S. N.; Kestner, R. *Phys. Rev. A* **1988**, *38*, 1111.
(50) Tatewaki, H.; Tomonari, M.; Nakamura, T. *J. Chem. Phys*. **1988**, *88*, 6419.
(51) Noro, T.; Ballard, C.; Palmer, M. H.; Tatewaki, H. *J. Chem. Phys.* **1994**, *100*, 452.
(52) Yanasigava, S.; Tsuneda, T.; Hirao, K. *J. Chem. Phys.* **2000**, *112*, 545.
(53) Barden, C. J.; Rienstra-Kiracofe, J. C.; Schaefer, H. F., III. *J. Chem. Phys.* **2000**, *113*, 690.
(54) Chen, J. L.; Wang, C. S.; Jackson, K. A.; Pederson, M. R. *Phys. Rev.* **1991**, *44*, 6558.
(55) Gutsev, G. L. *Phys. Rev. B* **2002**, *65*, 132417.
(56) Gutsev, G. L.; Khanna, S. N.; Jena, P. *Phys. Rev. B* **2000**, *62*, 1604.
(57) Leopold, D. G.; Lineberger, W. C. *J. Chem. Phys.* **1986**, *85*, 51.
(58) Gutsev, G. L.; Andrews, L.; Bauschlicher, C. W., Jr. *J. Chem. Phys.* Submitted.
(59) Rohlfing, E. A.; Cox, D. M.; Kaldor, A.; Johnson, K. H. *J. Chem. Phys.* **1984**, *81*, 3846.
(60) Sunderlin, L. S.; Wang, D.; Squires, R. R. *J. Am. Chem. Soc.* **1992**, *114*, 2788.
(61) Tremblay, B.; Manceron, L. Unpublished results.
(62) Bagus, P. S.; Hermann, K.; Bauschlicher, C. W., Jr. *J. Chem. Phys.* **1984**, *80*, 4378.
(63) Koutecky, J.; Pacchioni, G.; Fantucci, P. *Chem. Phys.* **1985**, *99*, 87.
(64) Moskovits, M.; Di Lella, D. P. *J. Chem. Phys.* **1980**, *73*, 4917.